J Mater Sci (2009) 44:3770–3776
DOI 10.1007/s10853-009-3506-8

Measurement of interfiber friction force for pulp fibers by atomic force microscopy

Fang Huang · Kecheng Li · Artem Kulachenko

Received: 17 December 2008 / Accepted: 18 April 2009 / Published online: 6 May 2009

Abstract Interfiber friction in paper exists in fiber suspensions, fiber flocs, and fiber networks. The interfiber friction force is, therefore, important both in papermaking and in the use of paper. The objective of this research is to develop a methodology using atomic force microscopy (AFM) for the direct measurement of the friction force between pulp fibers. Different factors such as AFM scanning velocity, contact area, and fiber surface roughness were investigated. The results show that AFM is an effective tool for measuring micro-scale interfiber friction forces. Both AFM scanning velocity and fiber surface roughness affect the measured results. The coefficient of friction increases, but the initial adhesion force decreases, with increasing fiber surface roughness.

Introduction

Friction is the force resisting the relative lateral motion of two solid surfaces in contact, or a solid surface in contact with a fluid. It is one of the oldest subjects in physics and is of great practical importance in many industrial operations. Friction between fibers in pulp or paper influences papermaking and paper use, such as the pulping process, paper machine runnability, and physical strength of paper [1]. Interfiber friction force is an important factor in holding together the fiber network structure, including the fiber suspension, fiber flocs, wet web, and final paper structure.

Friction between fiber and machine parts, as well as interfiber friction, have been the subject of many investigations [2–7]. Previous work on fiber friction has been carried out mostly by researchers in textile field. Lord [7] divided the field of fiber friction into three categories: friction between two single fibers; friction between a single fiber and a fiber assembly; and friction between fiber assemblies. Most of the investigations have focused on cotton and synthetic fibers. Two methods for measuring the interfiber friction have been reported [4, 8–10]. The first is the point contact method [8, 9], in which one fiber is rubbed perpendicular to another fiber. The second is the extended line contact method [10], in which two fibers are twisted together. By using the point contact method, Andersson et al. [4] determined the coefficient of friction for the sliding friction of rayon and natural cellulosic, such as Kraft pulp fiber and thermo-mechanical pulp fiber to be in the range of 0.50–0.60 in air-dry state. Lindberg [10] applied the extended line contact method and obtained a coefficient of friction of 0.35–0.40 between nylon fibers. Since pulp fibers have lengths on the order of a few millimeters, and width on the order of tens of micrometer in the friction force measurement, special procedures and complicated apparatus were developed in both of these two methods.

Macroscopic forces on a fibrous system are transmitted by the fibers in a complicated way, which makes a rigorous analysis difficult [4]. The atomic force microscope (AFM) has been used in recent years for friction studies [11–14]. The AFM applies very low load and very small motion, in micrometer scale, and make it possible to measure the interfiber friction force in fiber network [11]. In the

F. Huang (✉) · K. Li
Department of Chemical Engineering and Limerick Pulp and Paper Centre, University of New Brunswick, Fredericton E3B 6C2, NB, Canada
e-mail: fang@unb.ca

A. Kulachenko
Pulp and Paper Research Institute of Finland (KCL), P.O. Box 70, 02151 Espoo, Finland

measurement, the AFM tip scans the surface laterally and the lateral deflection signal is converted to interfacial friction force. However, the interfacial friction force is greatly influenced by the contact area between the AFM tip and the surface. The contact area is determined by several factors, such as applied force load, geometry of AFM tip, and the topography and elasticity of the sample surface. In order to minimize and simplify the effect of contact area, a model surfaces, i.e., nano-crystalline cellulose film [15–21], and functionalized AFM tips, such as geometrically defined cellulose sphere tip [15, 16, 18–20, 22, 23] were used in the AFM friction force measurement. However, none of these measurements were performed on real pulp fibers. Mizuno et al. [9], for the first time, made the friction measurement feasible between two polyester fibers with a scanning probe microscope (SPM). The key technique in this measurement was to attach the polyester fiber to the cantilever with epoxy glue (two-component epoxy, Araldit Rapid, Casco). Compared with polyester fiber, pulp fibers are very irregular both on the surface and in the cross-section. It is much more difficult to measure friction forces between pulp fibers than synthetic fibers.

The purpose of the present work is to develop a new method to measure the friction force between single pulp fibers by using AFM. Factors, such as tip scanning velocity, fiber surface roughness and real contact area were investigated.

Theory

The two basic laws of friction were first discovered by Leonardo da Vinci in 1500s, who stated that the friction force is proportional to the normal force, and that it is independent of the contact area [24]. These laws were rediscovered by Amontons in 1699 and he initially described the friction force as follows:

$$F = \mu N \tag{1}$$

where F is the friction force, μ is the coefficient of friction, and N is the normal force. These laws were further investigated in 1788 by Coulomb, who made the distinction between static and kinetic friction. The coefficients of friction describing static and kinetic friction have been found to be time and velocity dependent, respectively [25].

Several researchers [7, 26] have noticed deviations from Amontons's law; in particular in the friction force measurement by atomic force measurement. Therefore, an extra constant term, F_0, has been added to Amonton's law:

$$F = \mu_{F_0} N + F_0 \tag{2}$$

where constant F_0 is interpreted as an additional cohesive force (or initial adhesive force) and it is independent of normal force, μ_{F_0} is the modified coefficient of friction. F_0 is the friction force at zero normal force loads. The use of this method for the interpretation of micro-scale friction was proposed by Lord [7] and Carpick et al. [26].

Furthermore, it was found that the micro-scale friction was also affected by the contact area [27]. Since all surfaces of solid bodies are rough on microscale, the apparent area of contact is much larger than the true one, as contact occurs only at the surface asperities [28]. Homola [29] found that in sliding (shearing) of two molecularly smooth surfaces in liquids, the frictional force F_f is directly proportional to the contact area (A) and shear strength (τ), as shown in Eq. 3:

$$F_f = \tau A \tag{3}$$

Based on these findings, in the measurement of interfiber friction by using AFM, pulp fibers with rough surfaces are expected to contribute significantly to the coefficient of friction. In addition, the scanning velocity and the initial adhesive force may also affect the measurement.

Experimental

Materials and sample preparation

Commercial spruce TMP pulp was obtained from Finland. The Canadian standard freeness (CSF) freeness of this pulp is 360 mL (Tappi standard T-227 om-04). In order to study the effect of surface roughness on interfiber friction, fibers with different roughness were prepared by using PFI refining. The TMP pulp was further refined by a PFI mill at 10% consistency to get four freeness levels: 290, 250, 160, and 110 mL.

The pulp suspension (about 0.05 g/L) was deposited with a pipette on double-sided tape, prior to sticking it on the glass slide (Fisher brand precleaned microscope slide). The deposited fiber suspension was stored overnight at room temperature to evaporate the water. The fibers were then stuck on the double-sided tape for the AFM analysis.

AFM methodology

Basic principles and procedures in friction measurement by AFM

In friction force measurement, the surface is moved laterally with respect to the AFM cantilever, back and forth along a line. Friction causes the cantilever to twist in the direction opposite to the scanning direction, and this generates a lateral signal due to the difference in intensity between the right-hand and the left-hand motion. In this way friction loops can be recorded, as shown in Fig. 1,

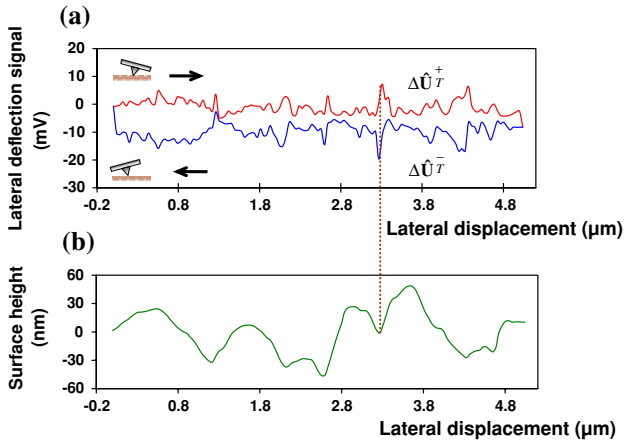

Fig. 1 Friction loop (**a**) and influence of topography on lateral signals (**b**)

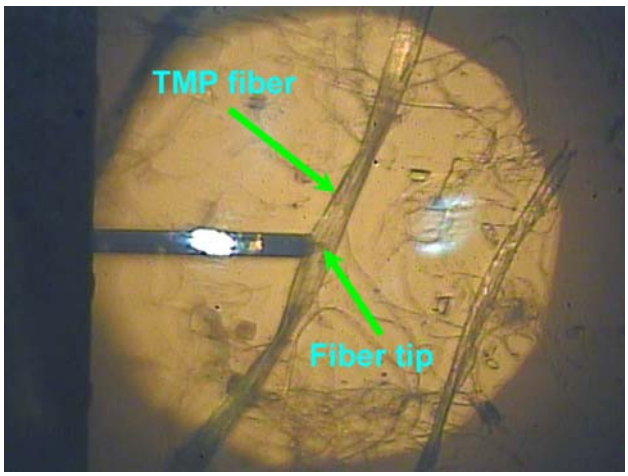

Fig. 2 AFM fiber tip is in contact with a TMP fiber

where the lateral deflection signal (V) is plotted against the lateral displacement of the sample. Figure 1 also shows that the topographic profile of the scanned line contributes to the lateral signal. This is due to the torsion of the cantilever when the tip encounters a step feature on the surface. The influence of topography on the lateral signal that is common to both scanning directions can be partly cancelled by calculating the average lateral signal, $\Delta\hat{U}$, based on the average lateral signals recorded during the trace, $\Delta\hat{U}_T^+$, and retrace, $\Delta\hat{U}_T^-$ [30, 31], as indicated in Eq. 4:

$$\Delta\hat{U} = \frac{\Delta\hat{U}_T^+ - \Delta\hat{U}_T^-}{2} \tag{4}$$

The average lateral signal ($\Delta\hat{U}$) in volts can be converted to force (F) by multiplying the lateral sensitivity of cantilever (S_X):

$$F = S_X \Delta\hat{U} \tag{5}$$

In this study, friction was measured using a MFP-3D AFM (AsylumResearch, USA). The fibers were brought into contact and a normal force curve was recorded (Fig. 2). This requires scanning in contact mode at a scan angle of 90° with the slow axis scan being disabled. The feature of slow scan disabled formed a "single line scan". Fiber surface is irregular and inhomogeneous [32], and a single line scan loop permits scanning with the same surface characteristics which minimizes the difference in sample surface under investigation. In order to reduce the influence of microfibril angle in the measurement [33], all the scans were parallel to the fiber length direction. Friction measurements were then performed starting at low applied loads, and increasing gradually the load after each friction loop. The scan size was 5 μm with scanning frequency of 0.5, 1.0, 1.5, and 2 Hz. Once the scanning was completed, the MFP-3D software generated the average friction force–load curve automatically. Friction coefficients were obtained by fitting the linear regions of the friction–load curve. For statistical purpose, at least 10 measurements were taken for each fiber sample. The reported friction coefficient is the average of the 10 measurements. All the measurements were done at room temperature (20–23 °C) and humidity (relative humidity: 35–45%).

Assembly of fiber probe

The fibers were washed with distilled water and dried before use. The fibers were randomly selected and cut to about 20 × 40 μm in size under an optical microscope. Fiber probes were prepared by attaching a fiber segment to the top of a Silicon Nitrate rectangle cantilever (400 × 35 μm) at Novascan (USA). The fiber attachment was operated by a multiple micro-manipulation apparatus which was designed specifically for the colloidal modification of AFM probes. The fiber segment was attached using a proprietary adhesive that has demonstrated resistance to organic solvents and extreme pH. This operation was carefully controlled to make the top surface of fiber segment free of adhesive. Figure 3 shows the assembly of a fiber probe. The spring constant was 0.03 N/m which was pre-calibrated by Novascan.

AFM calibration

The quantitative determination of friction forces by AFM requires the conversion of the output voltage signal of the sector area-sensitive photodiode to force. As discussed earlier, the friction force was calculated by multiplying the lateral deflection signal (V) and cantilever lateral sensitivity (S_X). The same principle was applied for the normal force (load) calculation, i.e., normal deflection signal (S_Z) multiplied by the cantilever sensitivity equals the normal force (load). The normal sensitivity was calibrated by the

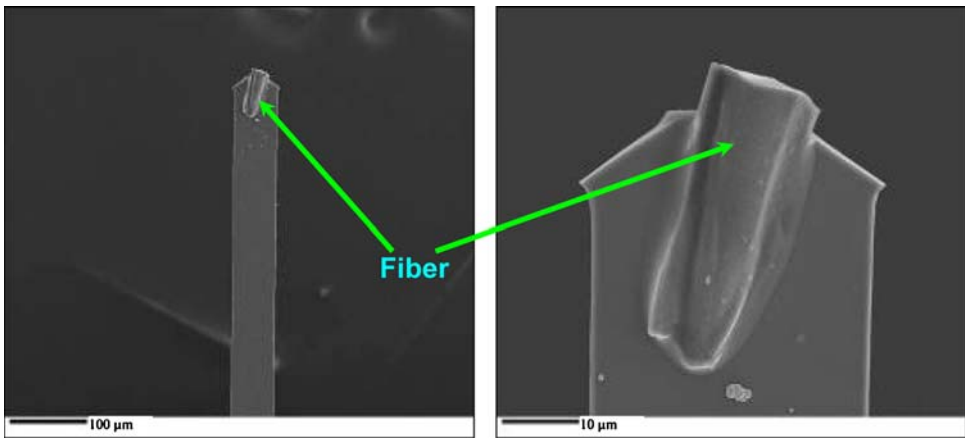

Fig. 3 A segment of fiber is attached on cantilever

MFP-3D standard Thermal tune method [34]. However, the lateral sensitivity calibration was more complicated. Several existing methods produce large errors and give poor reproducibility. In this investigation, a wedge calibration method was adopted in the calculation [35]. Among the numerous methods, this method is probably the most robust and accurate method so far and is also the most commonly accepted [36–38]. In this approach, the cantilever is scanned across a wedge calibration grating TGF11 (Mikro Masch), and the friction signal is measured as a function of applied load. This lateral sensitivity (S_X) calibration is carried out automatically with the MFP-3D software. In this study, the normal sensitivity (S_Z) and lateral sensitivity (S_X) of fiber tip obtained are 4.16 and 564.25 nN/V, respectively.

Results and discussion

Friction–load curve

Figure 4 shows a typical interfiber friction force as a function of normal load. It was for a pulp fiber of CSF 250 mL at scanning rate of 1 Hz. The friction force increases quite linearly with the increase of normal load. The coefficient of friction value was obtained as the slope of the best linear line fit of the plot. It can also be seen that the friction force exists even at the zero applied normal load. This is mainly attributed to the influence of intrinsic adhesion force which is also referred to as initial adhesion force F_0 [39, 40]. The initial adhesion force is mainly due to the contribution of various attractive forces, such as capillary, electrostatic, van der Waals force, and chemical bonding under different circumstances [41]. In fiber–fiber contact, it was suggested that the capillary force is the major contribution to the adhesion force owning to its hydrophilic nature [42]. Condensation of water from the environment is the origin of capillary force that leads to the formation of meniscus bridge between the tip and sample [42].

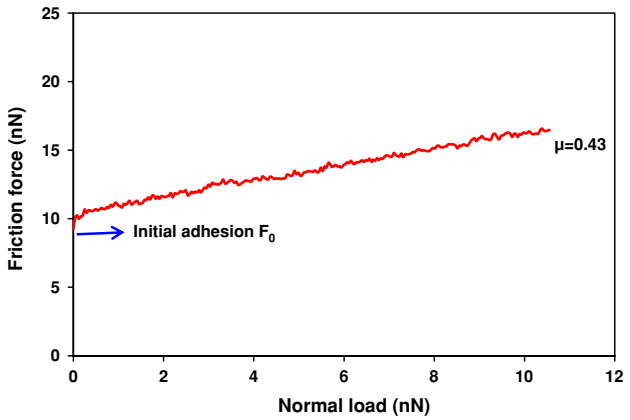

Fig. 4 Friction–load curve

Effect of scanning velocity

The observed friction versus scanning velocity behaviour for the tested samples is summarized in Fig. 5. For all the samples, the sliding speed dependence on the friction force was studied for a normal load of 10 nN with pulp fiber of CSF 250 mL. For interfiber contact, the coefficient of friction decreases from 0.47 to 0.39 with increasing the sliding speed. This behaviour is caused by the change in capillary action with sliding speed. Higher sliding speeds

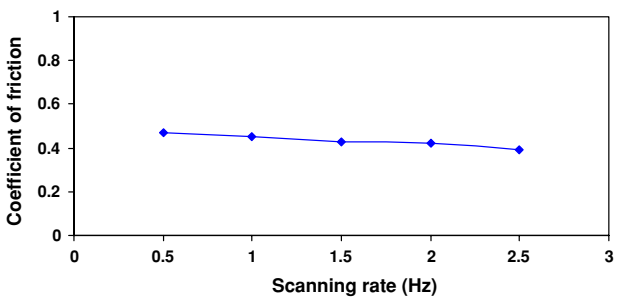

Fig. 5 Effect of scanning velocity on coefficient of friction

prevent the system from forming a stable capillary meniscus between fibers [43]. On the other hand, high sliding rate also cause high interface temperatures, which may reduce the viscosity of water, leading to a drop in the coefficient of friction [44, 58]. Due to the effect of capillary action, the reported dependence of scanning velocity on microfriction is more sensitive in humid environment than in dry environment [44].

It can be seen from Fig. 5 that the coefficient of friction does not change significantly with the increase of scanning rate. Therefore, only the scanning rate of 1 Hz was used in the other tests.

Effect of contact area

As discussed earlier, friction in microscale is also related to the real area of contact (A). In this study, the effect of interfiber contact area on friction force was extensively investigated. The real contact area in friction sliding was estimated by the Johnson–Kendall–Roberts (JKR) model [45], assuming that the fiber–fiber contact at nanoscale is a pseudo-single asperity contact [46]. As described in JKR model: in short range contact, the pull-off (adhesion) surface force (F_{JKR}) between two spherical particles is given by Eq. 6:

$$F_{\mathrm{JKR}} = \frac{3}{2}\pi R\gamma \tag{6}$$

where γ is the effective solid surface energy and R is the reduced radius of curvature of the two surfaces. In the friction force measurement, the initial adhesion force F_0 was taken as the pull-off force F_{JKR}. According to this model, at zero load, the contact radius a_0 was given by Eq. 7:

$$a_0 = \left(\frac{6\pi\gamma R^2}{K}\right)^{1/3} \tag{7}$$

where K is the combined elastic modulus of tip and sample. In this case, since the tip and sample are the same types of fibres, it can be estimated as the fiber elastic modulus.

The variation of real contact radius a with normal load N is described by a relatively simple Eq. 8 [47]:

$$a = a_0 \times \left(\frac{1+\sqrt{1+N/F_{\mathrm{JKR}}}}{2}\right)^{2/3} \tag{8}$$

Assuming the tip is axially symmetric, the contact area A is simply given by Eq. 9:

$$A = \pi a^2 \tag{9}$$

By combining the Eqs. 6–9, if the γ and K are already known, the real contact area A can be obtained. An estimated $\gamma = 35$ mJ/m^2 was adopted for TMP fiber surface energy [48, 49] and a reduced elastic modulus $K = 10$ GPa was used in this calculation [50–54]. In an attempt to learn more about the relationship of the friction force and the area of contact, we plotted friction force versus the real contact area for the fiber sample (CSF 250 mL), and the result is shown in Fig. 6. It can be seen that the friction force increases with the contact area, which is in agreement with previous studies [42, 55]. However, the relationship between friction force and real contact area over the entire range of contact are not totally linear. The possible explanation for the deviation may be that the interfiber contact is not an ideal single-pseudo asperity contact, which is assumed in JKR model for the contact area calculation. Fiber surface is extremely rough and the interfiber contact is more complicated than the single asperity contact.

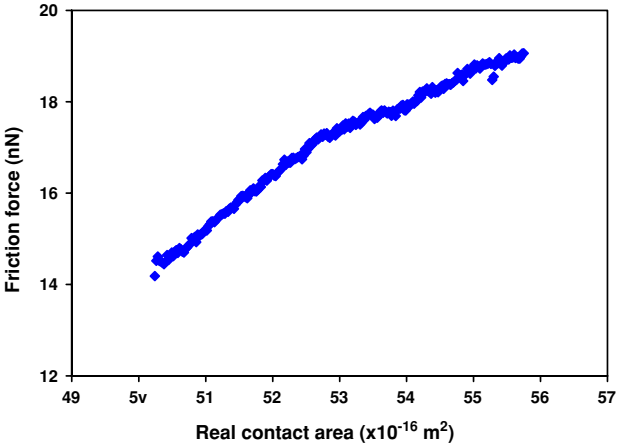

Fig. 6 Effect of contact area on friction force

Effect of surface roughness

In refining, the fiber surface roughness is increased by external fibrillation and delamination, which are favorable for the improvement of fiber surface specific area, interfiber friction and bonding [56–58]. In AFM analysis, surface roughness is most commonly characterized by the standard deviation of surface heights (Z value), which is the square root of the arithmetic average of squares of the vertical deviation of a surface profile from its mean plane. It is called root mean square surface roughness [59]:

$$R_{\mathrm{rms}} = \sqrt{\frac{\sum_{i=1}^{N}\left(Z_i - Z_{\mathrm{avg}}\right)^2}{N}} \tag{10}$$

where Z_{avg} is the average of the Z values within the given area, Z_i is the Z value of point i, and N is the number of points within the given area. Each RMS value presented is an average of 20 measurements from different fibers.

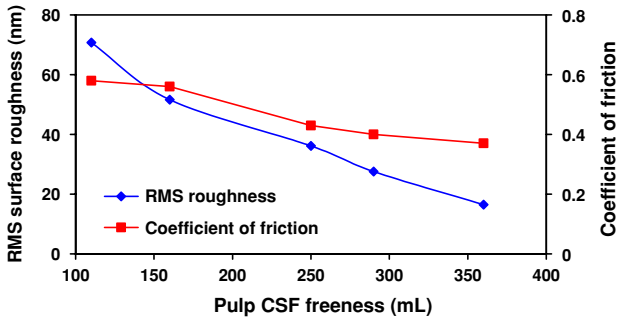

Fig. 7 Effect of refining on fiber surface roughness and interfiber friction

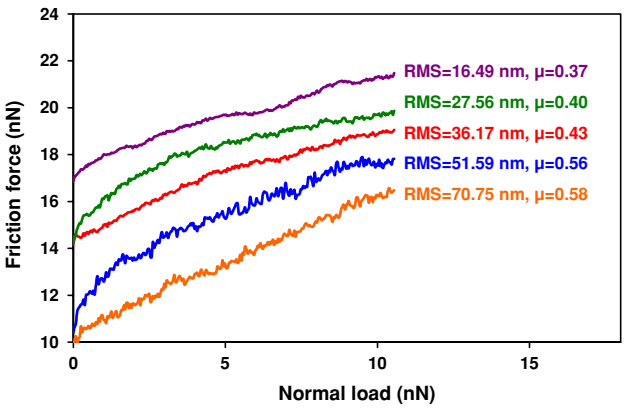

Fig. 8 Effect of RMS roughness on coefficient of friction and initial adhesion

Figure 7 shows the effect of refining on the fiber surface roughness and interfiber coefficient of friction. With the increase of refining, pulp freeness decreases from 360 to 110 mL and fiber RMS surface roughness increases from 16.49 to 70.75 nm. As a result, the interfiber coefficient of friction also increases from 0.40 to 0.51.

The correlation of the variation of coefficient of friction with that of surface roughness can be explained by the model developed by Bhushan [60]. In this model, the adhesive mechanism was assumed to be unchanged during sliding, and the local value of as so-called true coefficient of friction, μ_0, remains constant. When a sharp asperity (AFM tip) passes over a symmetrical single point asperity, i.e., rough surface, the average value of this coefficient of friction (μ_{avg}) can be calculated:

$$\mu_{\text{avg}} = \frac{\mu_0(1+\tan^2\theta)}{1-\mu_0\tan^2\theta} \tag{11}$$

where μ_0 is the true coefficient of friction between the sliding sharp asperity and the smooth surface, θ is the slope angle of the asperities with a horizontal plane. If the value of $\mu_0\tan\theta$ is small, Eq. 11 can be written as:

$$\mu_{\text{avg}} \approx \mu_0\left(1+\tan^2\theta\right) \tag{12}$$

Evidently, μ_{avg} for a rough surface is higher than μ_0 for a smooth surface.

Figure 8 shows a series of friction–load curves for different TMP pulp fibers with different surface roughness ranging from 16.49 to 70.75 nm. It can be seen that the coefficient of friction between TMP fibers is in the range of 0.40–0.60, which is in agreement with previous studies using other methods for friction measurement [4, 61–63].

The effect of RMS roughness on the interfiber coefficient of friction was also clearly shown in Fig. 8. It can be seen that under the same normal load, the increase of RMS surface roughness results in the increase of coefficient of friction. It is interesting to note that, under zero normal load, the friction force, or initial adhesion F_0, decreases with increasing of fiber surface roughness. For example, a higher roughness fiber (70.75 nm) has a lower interfiber initial adhesion force (9.63 nN) compared with a higher initial adhesion force (16.86 nN) obtained for a lower surface roughness (16.49 nm). Reduction of adhesion forces associated with nanoscale roughness is believed to be related to the decrease in the true contact area between a particle and a surface, and an increase in the distance between the surfaces [58, 64–67]. Mate [66] suggested the increase in distance between surfaces causes decrease in Van der Waals force between rough surfaces.

Conclusions

A new method for measuring the interfiber friction force has been developed using AFM. In this method, a modified fiber AFM tip was assembled to study the interfiber contact and interfiber friction force.

Results show the coefficient of friction between TMP fibers is in the range of 0.40–0.60, which is in agreement with previous studies. AFM scanning velocity affects measured friction force. Fiber surface roughness affects both friction force and initial adhesion force. Rough surface increases the coefficient of friction but decreases the initial adhesion.

Acknowledgements The authors would like to acknowledge the financial support of Atlantic Innovation Fund (AIF), Canadian Foundation for Innovation (CFI), and KCL (Finland) for this research work.

References

1. Back E (1991) Paper-to-paper and paper-to-metal friction. In: TAPPI international paper physics conference, Kona, Hawaii, pp 49–65
2. Mogahzy EYE, Gupta BS (1993) Textile Res J 63(4):219
3. Jong DHG (1993) Textile Res J 63(1):14
4. Andersson SR, Rasmuson A (1997) J Pulp Paper Sci 23(1):J5

5. Postle LJ, Ingham J (1952) J Text Inst Trans 43:T77
6. Cox DR (1952) J Text Inst 43:T87
7. Lord E (1955) J Text Inst 46:P41
8. Howell HG (1954) J Text Inst 45:T575
9. Mizuno H, Kjellin M, Nordgren N, Petterson T, Wallqvist V, Fielden M, Rutland MW (2006) Aust J Chem 59:390
10. Linderberg J, Gralén N (1948) Textile Res J 18(5):287
11. Srivastava A, Astrom KJ, Turner KL (2007) Tribol Lett 27:315
12. Perry SS, Somorjai GA, Mate MC, White RL (1995) Tribol Lett 1:233
13. Heim LO, Blum J, Preuss M, Butt HJ (1999) Phys Rev Lett 83(16):3328
14. Bhushan B (1998) Proc Inst Mech Eng Part J 212:1
15. Zauscher S, Klingenberg DJ (2001) Colloids Surf A: Physicochem Eng Aspects 178:213
16. Nigmatullin R, Lovitt R, Wright C, Linder M, Nakari-Setälä T, Gama M (2004) Colloids Surf B: Biointerfaces 35:125
17. Kontturi E, Tammelin T, Österberg M (2006) Chem Soc Rev 35:1287
18. Stiernstedt J, Nordgren N, Wågberg L, Brumer H, Gray DG, Rutland MW (2006) J Colloid Interface Sci 303:117
19. Stiernstedt J, Brumer H, Zhou Q, Teeri TT, Rutland MW (2006) Biomacromolecules 7(7):2147
20. Carambassis A, Rutland MW (1999) Langmuir 15(17):5584
21. Fält S, Vesterlind EL, Larsson PT (2004) Cellulose 11:151
22. Bowen WR, Stoton JAG, Doneva TA (2002) Surf Interface Anal 33:7
23. Feiler A, Larson I, Jenkins P, Attard P (2000) Langmuir 16(26):10269
24. Howell HG, Mieszkis KW, Tabor D (1959) Friction in textile. Butterworth Scientific Publications, London
25. Rabinowicz E (1995) Friction and wear of materials. John Wiley, New York
26. Carpick RW, Agraït N, Ogletree DF, Salmeron M (1996) J Vac Sci Technol B 14(2):1289
27. He JH, Batchelor WJ, Johnston RE (2007) J Mater Sci 42(2):522. doi:10.1007/s10853-006-1146-9
28. Bhushan B (1999) Principles and applications of tribology. Wiley-Interscience, New York
29. Homola AM, Israelachvili JN, Gee ML, McGuiggan PM (1989) J Tribol 111(4):675
30. Labardi M, Allegrini M, Ascoli C, Ferdiani C, Salerno M (1995) In: Guntherodt HJ, Anselmetti D, Meyer E (eds) Forces in scanning probe methods. Academic Publishers, Dordrecht, p 319
31. Sundararajan S, Bhushan B (2000) J Appl Sci 88(8):4825
32. Batchelor WJ, He J, Sampson WW (2006) J Mater Sci 41(24): 8377. doi:10.1007/s10853-006-0889-7
33. Entwistle KM, Kong K, MacDonald MA (2007) J Mater Sci 42(17):7263. doi:10.1007/s10853-006-1460-2
34. Hutter JL, Bechhoefer J (1993) Rev Sci Instrum 64:1868
35. Feiler A, Attard P, Larson I (2000) Rev Sci Instrum 71(7):2746
36. Ogletree DF, Carpick RW, Salmeron M (1996) Rev Sci Instrum 67(9):3298
37. Tocha E, Schonherr H, Vancso GJ (2006) Langmuir 22(5):2340
38. Varenberg M, Etsion I, Halperin G (2003) Rev Sci Instrum 74:3362
39. Bhushan B, Kulkarni AV (1996) Thin Solid Films 278:49
40. Yoshizawa H, Chen Y-L, Israelachvili J (1993) J Phys Chem 97: 4128
41. Maboudian R, Howe RT (1997) J Vac Sci Technol B 15(1):1
42. Bhushan B, Sundararajan S (1998) Acta Mater 46(11):3793
43. Liu HS, Ahmed I-U, Scherge M (2001) Thin Solid Films 381:135
44. Koinkar VN, Bhushan B (1996) J Vac Sci Technol A 14(4):2378
45. Johnson KL, Kendall K, Roberts AD (1971) Proc R Soc Lond A 324:301
46. Yoon E-S, Singh RA, Oh H-J, Kong H (2005) Wear 259:1424
47. Carpick RW, Ogletree DF, Salmeron M (1999) J Colloid Interface Sci 211:395
48. Gellerstedt F, Gatenholm P (1999) Cellulose 6:103
49. Kazayawoko M, Balatinecz JJ, Matuana LM (1999) J Mater Sci 34:6189. doi:10.1023/A:1004790409158
50. Yan D, Li K (2008) J Mater Sci 43:2869. doi:10.1007/s10853-007-2085-9
51. Neagu RC, Gamstedt EK (2007) J Mater Sci 42(24):10254. doi: 10.1007/s10853-006-1199-9
52. Ntenga R, Beakou A, Ateba JA (2008) J Mater Sci 43(18):6206. doi:10.1007/s10853-008-2925-2
53. Orso S, Wegst UGK, Arzt E (2006) J Mater Sci 41(16):5122. doi: 10.1007/s10853-006-0072-1
54. Davies P, Morvan C, Sire O (2007) J Mater Sci 42(13):4850. doi: 10.1007/s10853-006-0546-1
55. Bhushan B, Dandavate C (2000) J Appl Phys 87(3):1201
56. Page DH, Baker CF, Punton VW (eds) (1989) Fundamentals of papermaking. Mechanical Engineering Publications Ltd, London
57. Mohlin UB, Miller J (1995) Industrial refining effects of refining conditions on fibre properties. In: Proc. 3rd international refining conference, vol 4. Atlanta, March 19–22, p 1
58. Koinkar VN, Bhushan B (1997) J Appl Phys 81(6):2472
59. Mahlberg R, Niemi HE-M, Denes FS, Rowell RM (1999) Langmuir 15:2985
60. Bhushan B (1995) Handbook of micro/nanotribology. Chemical Rubber, Boca Raton, FL
61. Schmid CF, Klingenberg DJ (2000) J Colloid Interface Sci 226:136
62. Switzer LH, Klingenberg DJ (2004) Int J Multiphase Flow 30:67
63. Amelina EA, Shchukin ED, Parfenova AM, Bessonov AI, Videnskii IV (1998) Colloid J 60(5):537
64. Rabinovich YI, Adler JJ, Ata A, Singh RK, Moudgil BM (2000) J Colloid Interface Sci 232:10
65. Rabinovich YI, Adler JJ, Ata A, Singh RK, Moudgil BM (2000) J Colloid Interface Sci 232:17
66. Mate CM (1993) Wear 168:17
67. Fuller KNG, Tabor D (1975) Proc R Soc Lond A 345:327